applied sciences

MDPI

Article

Experimental Study on Fluid Dissipation Effects in Core Samples by NMR Measurement

Zhongshu Liao [1,2], Gong Zhang [1,2,*] and Yingying Ma [1,2]

[1] Key Laboratory of Oil and Gas Resources and Exploration Technology, Ministry of Education, College of Geophysics and Petroleum Resources, Yangtze University, Wuhan 430102, China; 2022710389@yangtzeu.edu.cn (Z.L.); 2022710371@yangtzeu.edu.cn (Y.M.)

[2] MRT&A Magnetic Resonance Technology and Application Laboratory, Yangtze University, Wuhan 430102, China

* Correspondence: zhanggong@yangtzeu.edu.cn

Abstract: Laboratory core nuclear magnetic resonance (NMR) relaxation measurements offer geological information, including rock porosity and oil saturation, relevant to logging. When core samples drilled from wells are exposed to air, the fluids within their pores inevitably dissipate. This phenomenon may lead to discrepancies between the results of nuclear magnetic resonance relaxation experiments and the actual situation underground. To deeply explore the impact of fluid dissipation on NMR core analysis experimental results, a series of simulated dissipation experiments were designed under constant temperature and humidity conditions. Variations in one-dimensional and two-dimensional NMR measurement results of oil-saturated samples were examined under varying crude oil viscosities and dissipation times. The experimental results indicate that as exposure time increases, the T_2 distribution of oil-saturated cores decreases, and the amplitude of the T_2 distribution peaks decreases. Both oil and water relaxation components show a decreasing trend; however, the dissipation rate of the bounding water component significantly exceeds that of the crude oil component. By employing two-dimensional NMR relaxation time distribution fluid quantitative analysis technology, the relationship between the dissipation rates of various phase fluids and exposure time during the stable dissipation stage was analyzed. This offers a reference for adjusting the oil saturation of exposed cores based on NMR measurements.

Keywords: core analysis; T_1-T_2; fluid dissipation; crude oil viscosity

Citation: Liao, Z.; Zhang, G.; Ma, Y. Experimental Study on Fluid Dissipation Effects in Core Samples by NMR Measurement. *Appl. Sci.* **2024**, *14*, 10746. https://doi.org/10.3390/app142210746

Academic Editor: Nikolaos Koukouzas

Received: 28 October 2024
Revised: 17 November 2024
Accepted: 18 November 2024
Published: 20 November 2024

1. Introduction

In the domain of oil exploration and development, oil and gas reserves serve as a crucial indicator of the outcomes of oilfield exploration. Parameters such as porosity and oil saturation are essential for evaluating the physical properties of formations and their associated reserves [1]. Numerous methods exist for calculating these essential parameters. The Archie equation is the most widely utilized method for calculating oil saturation [2]. The Archie equation determines rock saturation and evaluates reservoir oil potential by measuring core porosity, resistivity, and fluid resistivity. However, its reliance on specific assumptions and sensitivity to factors like rock uniformity and pore structure limit its applicability. To address these limitations, alternative methods have been explored [3,4], including NMR (nuclear magnetic resonance) technology. Unlike traditional approaches, NMR directly measures the hydrogen nuclear signal in formations and remains unaffected by rock skeleton and lithology [5]. This enables the precise determination of critical reservoir parameters, such as porosity [6], saturation, and permeability [7], offering a robust and accurate method for evaluating oil saturation.

With the increasing complexity of exploration targets, especially in unconventional reservoirs, traditional NMR technologies struggle to meet the demands for rapid and precise analysis [8]. NMR logging technology is constrained by the wellbore environment

and exhibits limited capability in distinguishing thin interlayers [9]. While laboratory NMR analysis achieves high measurement accuracy [10], it faces challenges such as small sample size, limited reservoir representativeness, lengthy measurement cycles, and inadequate timeliness. To address these, advancements such as mobile full-diameter core NMR scanning technology have been introduced [11], enabling immediate on-site measurements to improve timeliness [12,13]. However, even with this technology, cores inevitably experience exposure to air during sample handling and pretreatment, resulting in fluid dissipation within the pores. This time delay, often spanning minutes to hours, remains a challenge for accurately capturing the fluid distribution during NMR analysis. The impact of pore fluid dissipation on the results of nuclear magnetic resonance experiments warrants in-depth study. To investigate the specific impact of core dissipation time on NMR measurement results, this article analyzes the dissipation process of pore fluid in sandstone cores through physical simulation experiments. Furthermore, it obtains the dissipation rates of different fluid components through one-dimensional and two-dimensional NMR experimental monitoring of cores at various dissipation stages. The dissipation rate of bounding water is markedly higher than that of crude oil, leading to a significant increase in oil saturation. After the core is exposed to air for a period of time, it is observed that the T_2 values of crude oil components decrease, while the T_1/T_2 ratio markedly increases. These conclusions can serve as a reference for the accurate calculation of reservoir parameters.

2. Principles of NMR Core Experiments

NMR technology is a crucial method for acquiring core porosity and fluid type information. In a static magnetic field, the spin orientations of hydrogen nuclei are arranged randomly. When an external magnetic field is applied, the hydrogen nuclei undergo precession in the direction of the magnetic field, generating a magnetization vector. Applying a horizontal pulse sequence rotates the magnetization vector to a horizontal orientation. Once the external pulse sequence is removed, the magnetization vector gradually returns to its original orientation in a process referred to as relaxation. Relaxation time is categorized into longitudinal relaxation time T_1 and transverse relaxation time T_2 [14]. In NMR core analysis experiments, the transverse relaxation time is typically measured. The resulting one-dimensional T_2 distribution data can estimate the pore size distribution in the sample and identify the fluid types present within the pores [15]. As target reservoirs become increasingly complex and with advancements in NMR experimental technology, NMR core analysis has evolved from one-dimensional T_2 distribution measurements to two-dimensional distribution. Two-dimensional nuclear magnetic resonance leverages the coupling relationship between T_1 and T_2 to generate the T_1-T_2 two-dimensional distribution [16], allowing fluid components that overlap at T_2 to be distinguished at T_1, thereby enhancing fluid identification capabilities compared to one-dimensional methods [17,18].

2.1. T_2 Measurement

Transverse relaxation time T_2 is typically measured using the CPMG spin echo method. Initially, a 90° pulse is transmitted, followed by a series of 180° pulses at specified intervals to create a pulse sequence for measuring T_2. The echo amplitude measured using the CPMG pulse sequence exhibits multi-exponential decay over time, as represented by Equation (1):

$$b_i = \sum_{j=1}^{m} f(T_{2j}) exp\left(-\frac{t_i}{T_{2j}}\right), \quad (1)$$

where b_i is the echo amplitude at time t_i; T_{2j} is the j-th transverse relaxation time; and $f(T_{2j})$ is the amplitude corresponding to the j-th transverse relaxation time. By inverting Equation (1), we obtain $f(T_{2j})$, the T_2 distribution. For samples saturated with a single fluid, the T_2 distribution represents the pore size distribution: the longer the T_2 relaxation time, the larger the corresponding pore size. Measuring the transverse relaxation time T_2 of

core samples, in conjunction with the difference in T_2 distribution, and enhanced diffusion methods, facilitates the identification of fluid types within the samples [19].

In porous media, the transverse relaxation time of the fluid in the pores consists of three relaxation processes, represented by the following formula:

$$\frac{1}{T_2} = \frac{1}{T_{2B}} + \frac{1}{T_{2S}} + \frac{1}{T_{2D}}, \tag{2}$$

where T_{2B} is the bulk relaxation time, T_{2S} is the surface relaxation time, and T_{2D} is the diffusion relaxation time.

Bulk relaxation (T_{2B}) refers to the inherent relaxation mechanism of fluids within the pores of porous media, where the relaxation rate depends solely on the physical properties of the fluid. Surface relaxation (T_{2S}) is governed by the pore size of the porous media. When fluid molecules approach the pore surface, they interact with the solid surface, accelerating the relaxation of the fluid's magnetization vector. Surface relaxation significantly influences the distribution of T2 relaxation times in NMR measurements. It is expressed as:

$$\frac{1}{T_{2S}} = \rho \frac{S}{V}, \tag{3}$$

where ρ represents the surface relaxation rate of the rock [20], S denotes the total surface area of the rock pores, and V represents the pore volume.

Diffusion relaxation primarily depends on magnetic field non-uniformity and the diffusion behavior of fluid molecules [21] and is further influenced by factors such as pore size, pore shape, pore connectivity, and fluid properties. For small pore structures or complex pore networks, the diffusion relaxation effect is particularly pronounced and is expressed as:

$$\frac{1}{T_{2D}} = \frac{D(\gamma G T_E)^2}{12}, \tag{4}$$

where D represents the fluid diffusion coefficient, γ denotes the spin magnetic ratio, T_E is the echo interval, and G is the magnetic field gradient.

2.2. T_1-T_2 Measurement

When pore fluid components in the core are complex, T_2 spectrum signals may overlap, making it difficult for one-dimensional NMR distribution to distinguish fluid signals. Therefore, two-dimensional NMR measurements (such as T_1-T_2 distribution) are required. T_1-T_2 two-dimensional NMR technology can simultaneously observe longitudinal relaxation time T_1 and transverse relaxation time T_2, thereby enhancing the accuracy of identifying and distinguishing pore fluid signals [15,16]. The primary methods for T_1-T_2 two-dimensional NMR measurements are the saturation recovery (SR-CPMG) and inversion recovery (IR-CPMG) methods. Both methods measure spin echo sequences under different waiting times, with the primary difference being the dynamic range of the magnetization vector in T_1 measurement. The SR method measures the dynamic range of the magnetization vector as $(0, M_0)$ (M_0 is the maximum net magnetization vector), while the IR method measures it as $(-M_0, M_0)$. The signal amplitude decay over time measured using the IR method follows Equation (5):

$$b_{is} = \sum_{j=1}^{m} \sum_{r=1}^{p} f_{j,r} \left(1 - 2 \cdot exp\left(-\frac{T_{ws}}{T_{1r}}\right)\right) exp\left(-\frac{t_i}{T_{2j}}\right) \tag{5}$$

where b_{is} is the echo amplitude at time t_i with a waiting time T_{ws}; m is the number of transverse relaxation times T_{2j}; p is the number of longitudinal relaxation times T_{1r}; $f_{j,r}$ is the distribution function for transverse relaxation time T_{2j} and longitudinal relaxation time T_{1r}. By performing a two-dimensional joint inversion of this equation, we obtain $f_{j,r}$ and thus the T_1-T_2 two-dimensional distribution [15].

3. Experimental Workflow

Following exposure to air, the fluid on the surface and within the saturated core begins to diffuse into the atmosphere. The flow and loss of fluids within the sample can be tracked and monitored using NMR experiments [22]. To systematically investigate the effects of varying dissipation times on sandstone NMR measurement results, the following experimental plan was developed.

3.1. Experimental Instruments, Materials, and Measurement Parameters

The experimental devices include a MesoMR12-06H-I NMR core analyzer (Niumag Analytical Instrument Corporation, Suzhou, China) (the instrument operates at a magnetic field strength of 0.25 T, the frequency commonly used in laboratory core nuclear magnetic resonance measurements, and features a high signal-to-noise ratio, exceptional accuracy, and rapid measurement speed), a LY-BH-50 vacuum pressurization saturation device (Jiangsu Lianyou Scientific Research Instrument Co., Ltd., Jiangshu, China), a UPCP-100 porosity and permeability measuring instrument (Jiangsu Lianyou Scientific Research Instrument Co., Ltd., Jiangsu, China), a CSC-12S centrifugal machine (Shanghai Luxiangyi Laboratory Instrument Co., Ltd., Shanghai, China) (the instrument features temperature control and can exert a 6.9 MPa displacement force, enabling rapid core dehydration), a milligram precision electronic balance, and NMR-specific sample tubes (Niumag Analytical Instrument Corporation, Suzhou, China).

The materials used consist of two processed sandstone core samples (labeled A and B) and crude oil of varying viscosities (42 mPas and 240 mPas). Additionally, plastic wrap and polytetrafluoroethylene (PTFE) film are employed for sample packaging.

Regarding the measurement parameters, the magnetic field strength of the NMR core analyzer used in the experiment is 0.25 T, corresponding to a resonance frequency of 12 MHz. The CPMG and IR-CPMG sequences are employed to collect T_2 distribution and T_1-T_2 two-dimensional distribution at different dissipation stages. T_2 distribution measurement parameters are set as follows: the number of echoes (NECH) is 12,000, the number of superpositions (SCAN) is 32, the echo interval (TE) is 0.1 ms, and the waiting time (TW) is 4000 ms. T_1-T_2 distribution measurement parameters are set as follows: the number of echoes (NECH) is 12,000, the number of superpositions (SCAN) is 16, the echo interval (TE) is 0.1 ms. The waiting times (TW) are as follows: 0.08 ms, 0.13 ms, 0.30 ms, 0.69 ms, 1.57 ms, 3.60 ms, 8.17 ms, 18.66 ms, 42.56 ms, 97.10 ms, 221.50 ms, 505.32 ms, 1152.82 ms, 2630.00 ms, and 6000.00 ms. The waiting time TW is set using a logarithmic uniform distribution with a base of ten. This approach spans multiple orders of magnitude, enabling the T1 relaxation time to correspond to different pore sizes and fluid properties. Additionally, it ensures an even distribution along the timeline. Using a linear interval would overly concentrate sampling points within a short time range, insufficiently describe the long time range, and reduce inversion accuracy. The dissipation exposure times for the core samples are set to 1 h, 2 h, 4 h, 8 h, 16 h, 32 h, 64 h, 96 h, 160 h, and 247 h to investigate the impact of different dissipation times on NMR measurement results.

3.2. Experimental Samples

The experimental samples are selected from sandstone cores obtained by drilling from Well Y in X oil field. These cores are pre-processed into standard 1-inch diameter cylindrical samples, as shown in Figure 1.

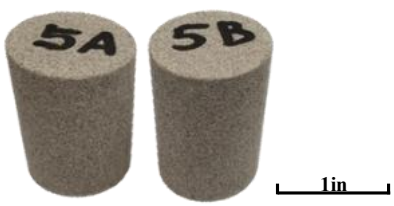

Figure 1. Photos of cores after cleaning and drying.

After cleaning and drying the cores, their weight and volume are measured. The porosity and permeability of the rock samples are measured using the helium method, as shown in Table 1.

Table 1. Basic parameters of experimental samples.

Sample	Volume (mL)	Dry Weight (g)	Helium Porosity (%)	Helium Permeability (mD)	NMR Porosity (%)	Oil Viscosity (mPas)
A	21.371	47.239	15.661	18.724	15.656	42
B	20.954	47.656	13.341	34.972	13.313	240

3.3. Experimental Steps

Cores A and B are evacuated in an environment of −0.1 MPa to remove gas, followed by the application of 20 MPa pressure for a duration of 10 days of water saturation treatment. After obtaining the water-saturated sample, a centrifuge is employed to further process the sample. Following the discharge of movable water from the sample, the two cores are saturated with oil separately to produce test samples in which bounding water and movable oil coexist, allowing for the monitoring of initial saturation. The degree of saturation is presented in Table 1. To minimize fluid loss during the measurement of the sample, plastic wrap is utilized to encase the core under analysis. After the measurement, the plastic wrap and PTFE are removed, and the exposed core is returned to the constant temperature and humidity chamber to simulate the dissipation process. The experimental process comprises the following steps:

(1) Check whether the instrument magnet temperature is stable, whether the main frequency is correct, and whether the 90-degree and 180-degree pulses are accurate.
(2) Set measurement parameters such as the number of echoes (NECH), the number of superpositions (SCAN), the echo interval (TE), and the waiting time (TW) according to the measurement requirements.
(3) Measure the NMR T_2 distribution and T_1-T_2 two-dimensional distribution of the processed core.
(4) Place the measured sample in a constant temperature and humidity chamber, setting the temperature to 25 °C and the humidity to 40% to simulate the dissipation process. Repeat step 3 at regular intervals throughout the experiment, with the time intervals set to 1, 2, 4, 6, 8, 16, 32, 64, 96, 160, 247 h.

4. Experimental Results

4.1. Fluid Dissipation Rate

During NMR measurements at various dissipation time points, the mass of the core samples is recorded using an electronic balance. As dissipation time increases, the weight of both core samples exhibits a downward trend, initially decreasing rapidly before gradually stabilizing (as illustrated in Figure 2). Notably, during the initial 100 h (as indicated by the dotted line in Figure 2), the weight of the cores significantly decreases as dissipation time increases. Subsequently, the change in core weight becomes significantly smaller and gradually stabilizes.

To eliminate the discrepancies in initial weight and volume of the cores, the decline in core weight over time is calculated and normalized based on sample volume, yielding the dissipation rate of fluid per unit volume of the core, as illustrated in Figure 3.

The unit volume dissipation rate reflects the rate of fluid dissipation. The curve in Figure 3 is divided into three stages: The first stage occurs within the initial two hours, as indicated by the first dotted line in Figure 3, during which the dissipation value per unit volume of the core fluid is maximized. This phenomenon is attributed to the fluid remaining on the core surface, which rapidly disperses into the air due to the large contact area. The second stage occurs from 2 to approximately 64 h of dissipation, as indicated by the second dotted line in Figure 3, during which the dissipation rate is relatively stable and

rapid. This stage likely involves the more easily dissipated fluid within the core rapidly escaping into the air through seepage channels. The third stage, referred to as the stable stage, occurs after 96 h, during which the fluid dissipation rate gradually decreases to a relatively stable low-value region. This stage represents the dispersal phase of movable oil, characterized by high oil viscosity and a significantly reduced dispersal rate. In the context of NMR core measurement technology, the second stage is the central focus of this research, characterized by a time distribution spanning from 2 to 96 h. This period corresponds to the interval during which the core is extracted from the wellbore and subsequently processed for measurement or further experimental analysis. During this critical phase, fluid changes within the core are most pronounced and exert the greatest influence on measurement results. These changes directly affect the accuracy and reliability of experimental data, making it essential to analyze the dissipation behavior of fluids during this stage comprehensively.

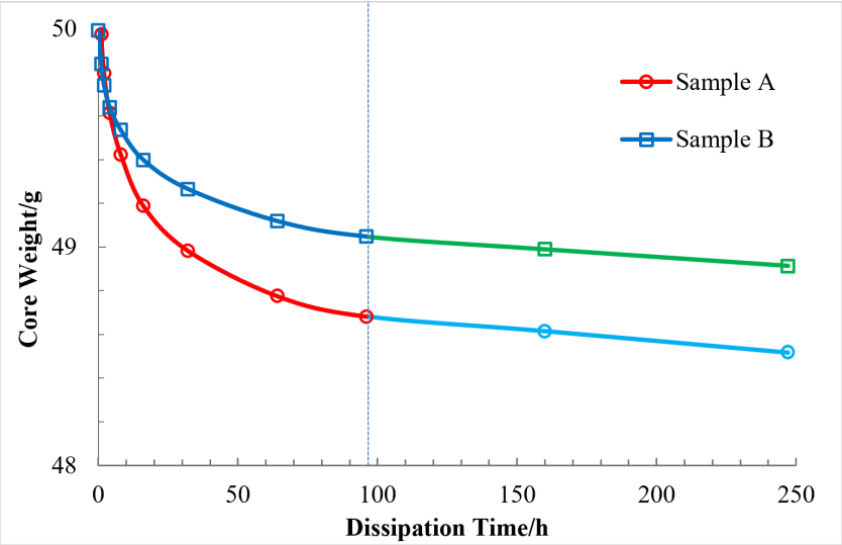

Figure 2. Mass change rate of sample A and sample B. Light blue and Green line represents the second stage of sample's dispersion.

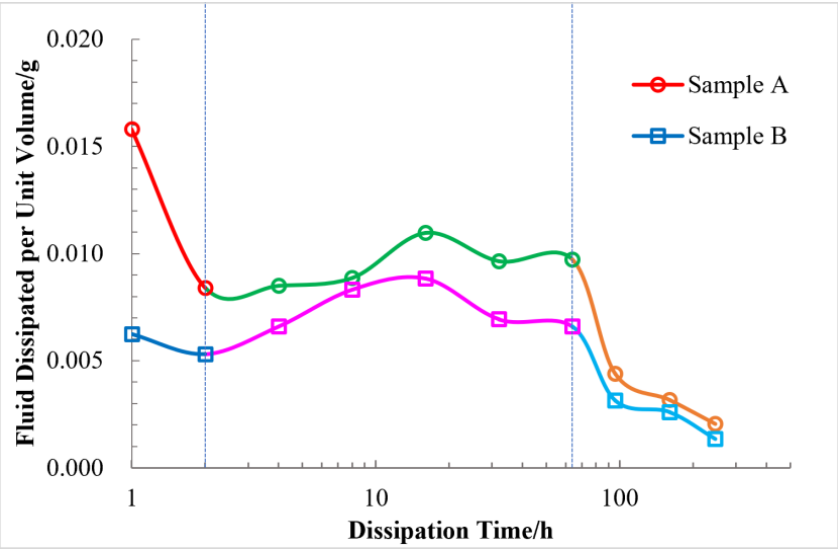

Figure 3. The rate of fluid change in sample A and sample B.

4.2. One-Dimensional NMR T_2 Distribution Measurement Results

The fluid content and composition within the rock core can be effectively determined by analyzing the area and morphology of the one-dimensional T_2 distribution. The total area under the T_2 distribution curve decreases as the fluid content in the rock core diminishes, reflecting the progressive dissipation of fluids. Moreover, distinct peaks within the T_2 distribution correspond to specific fluid components, such as bounding water and crude oil. Therefore, changes in the morphology of the T_2 distribution provide valuable insights into the fluid state of different components, enabling a detailed analysis of their dissipation behaviors and interactions within the pore structure. The T_2 distribution of the two core samples at various dissipation times are obtained through NMR measurements, as shown in Figure 4. The amplitudes of the T_2 distribution for both cores exhibit a gradual decline; however, the patterns of changes in the T_2 distribution differ significantly between the two cores. Due to the lower viscosity of oil in sample A, the two fluid components in sample A are more distinctly separated in terms of transverse relaxation time at the initial state, whereas those in sample B are harder to distinguish. Over time, however, the two fluid components gradually differentiate as the rapid evaporation of bound water causes the signal with shorter relaxation times to decrease more quickly, reducing the overlap between the two components.

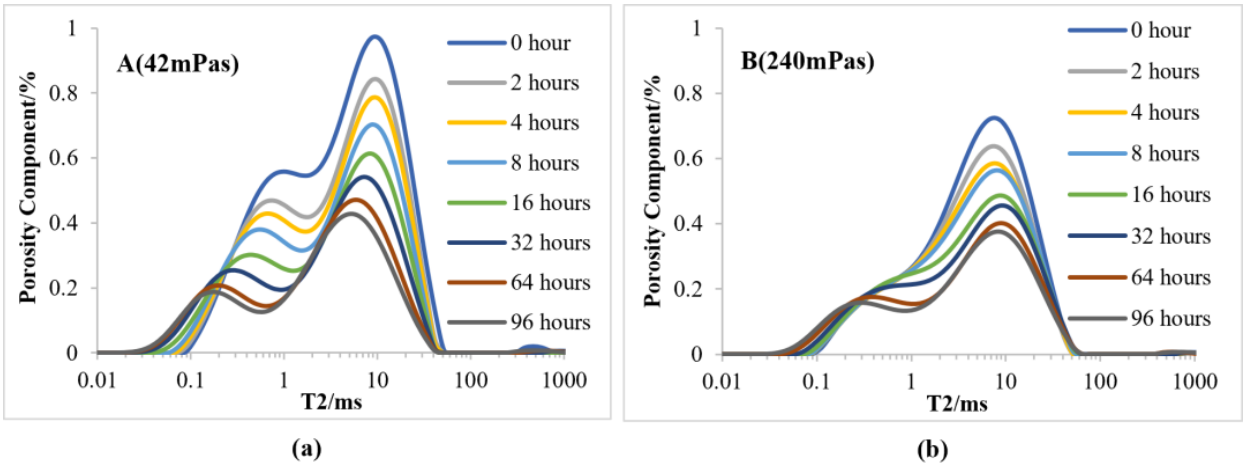

Figure 4. T_2 distribution measurement results at different dissipation stages: (**a**) T_2 relaxation time of sample A; (**b**) T_2 relaxation time of sample B.

Core A initially exhibits a bimodal feature, with the amplitude of the right peak significantly greater than that of the left peak. As dissipation progresses, the amplitudes of both peaks begin to decrease, exhibiting no significant difference in the rate of decline. Furthermore, as the amplitudes of the two peaks decrease, their T_2 distributions gradually decrease: the left peak shifts from 0.8 ms to approximately 0.15 ms, while the right peak shifts from 10 ms to 5 ms.

Core B initially does not display a clear bimodal feature, with the T_2 distribution ranging from 0.1 ms to 100 ms. During the oil-water dissipation process, the reduction in peak amplitude is distributed between 0.4 ms and 40 ms.

4.3. T_1-T_2 Two-Dimensional NMR Distribution Measurement Results

Two-dimensional NMR experimental results provide an intuitive means to distinguish fluid components in rock pores. Beginning with the initial saturation state of the core, the two main fluid components—bounding water and crude oil—within the pores can be distinctly identified, with bounding water situated in the lower left corner and crude oil in the upper right corner. Despite some overlap in the T_2 relaxation time direction, combining T_1 and T_2 dimensions allows for clear differentiation between the two, as shown in Figure 5. This primarily arises from the variations in T_1 and T_2 relaxation times among different

fluid types. Bounding water, due to its interaction with the rock surface, typically exhibits a shorter T_2 relaxation time, with T_2 distribution values generally falling in the range of 0.1–10 ms. Crude oil exhibits a relatively longer T_2 relaxation time compared to bounding water. The T_2 distribution values for crude oil range from 10–100 ms [16,23].

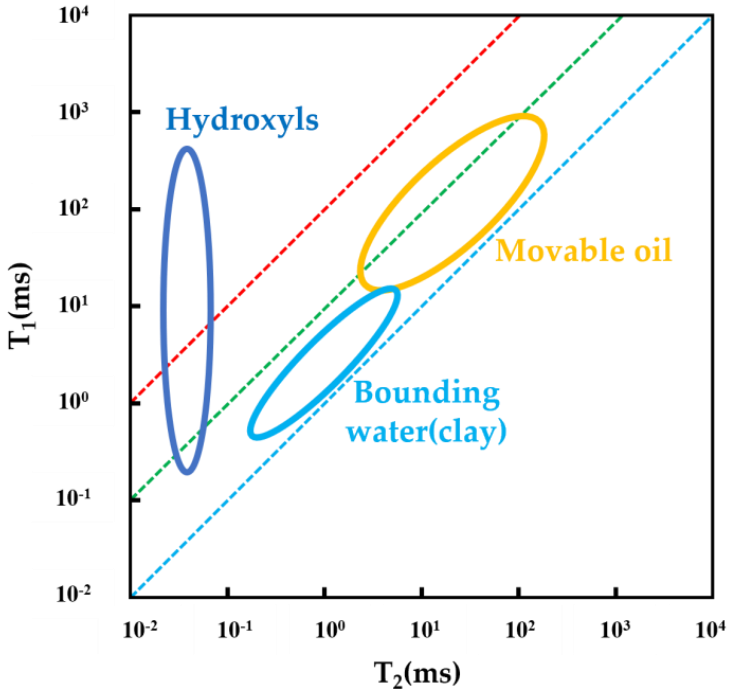

Figure 5. T_1-T_2 fluid identification plate (adapted from Fleury M, 2016 [24]).

Using Core A as the demonstration case, the NMR T_1-T_2 distribution at each dissipation time point are plotted on the same scale, as illustrated in Figure 6. The experimental results indicate that at the initial stage of fluid dissipation (as shown in Figure 6), the crude oil peak signal is located in the region of T_2 = 16.4 ms and T_1 = 67.2 ms, while the bounding water peak signal is located in the region of T_2 = 0.64 ms and T_1 = 2.4 ms. After two hours (as shown in Figure 6), a noticeable separation between the crude oil and bounding water signals is observed. As dissipation progressed, the separation between the two signals became more pronounced. After 247 h of dissipation (as shown in Figure 6), the crude oil peak signal shifts to the region of T_2 = 11.16 ms and T_1 = 51 ms, while the bounding water peak signal shifts to the region of T_2 = 0.14 ms and T_1 = 0.4 ms. In terms of signal strength, the amplitudes of both crude oil and bounding water gradually weaken with increasing dissipation time, with the strength of bounding water decreasing more significantly. After 247 h of dissipation, the bounding water signal nearly disappears.

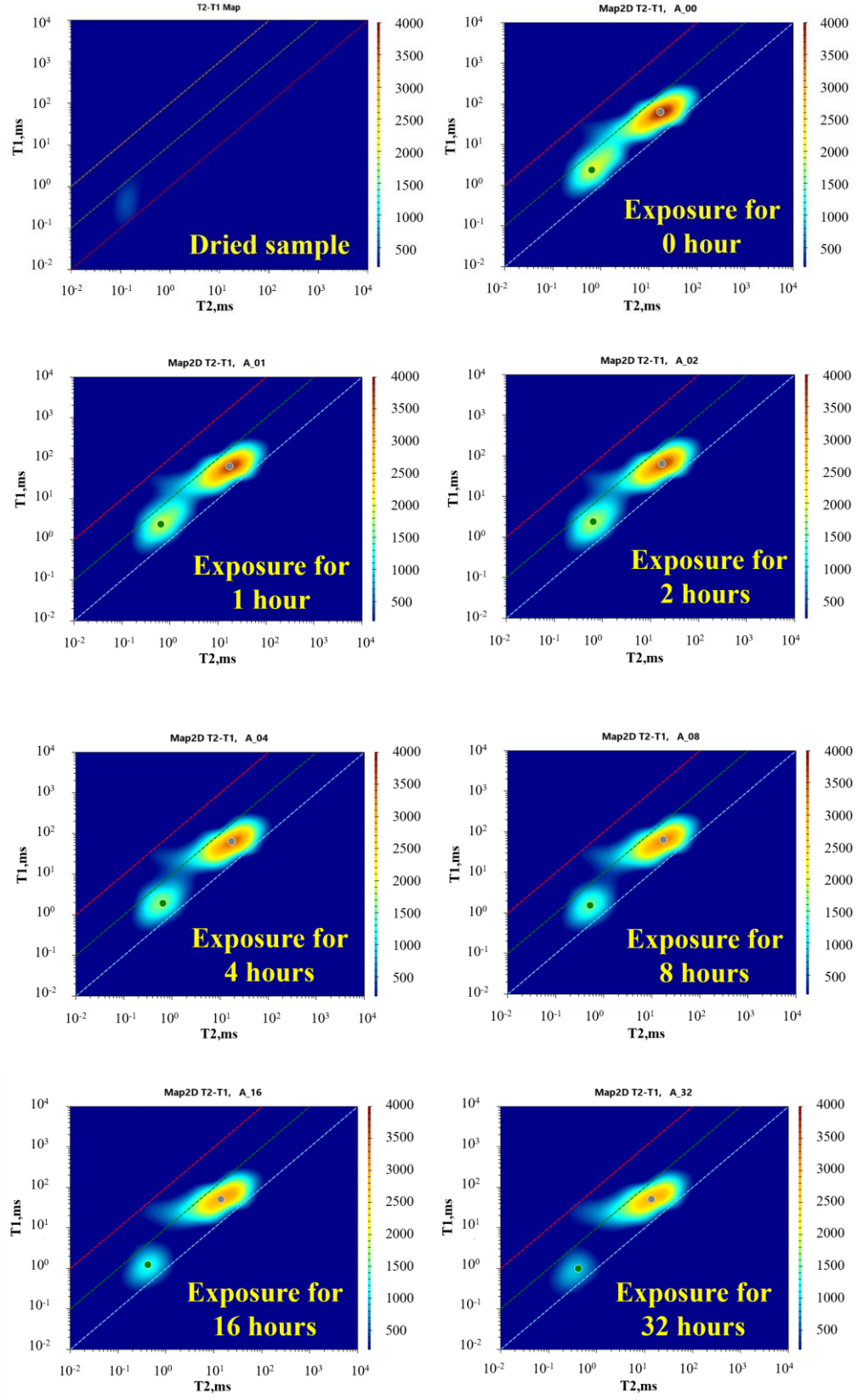

Figure 6. *Cont*.

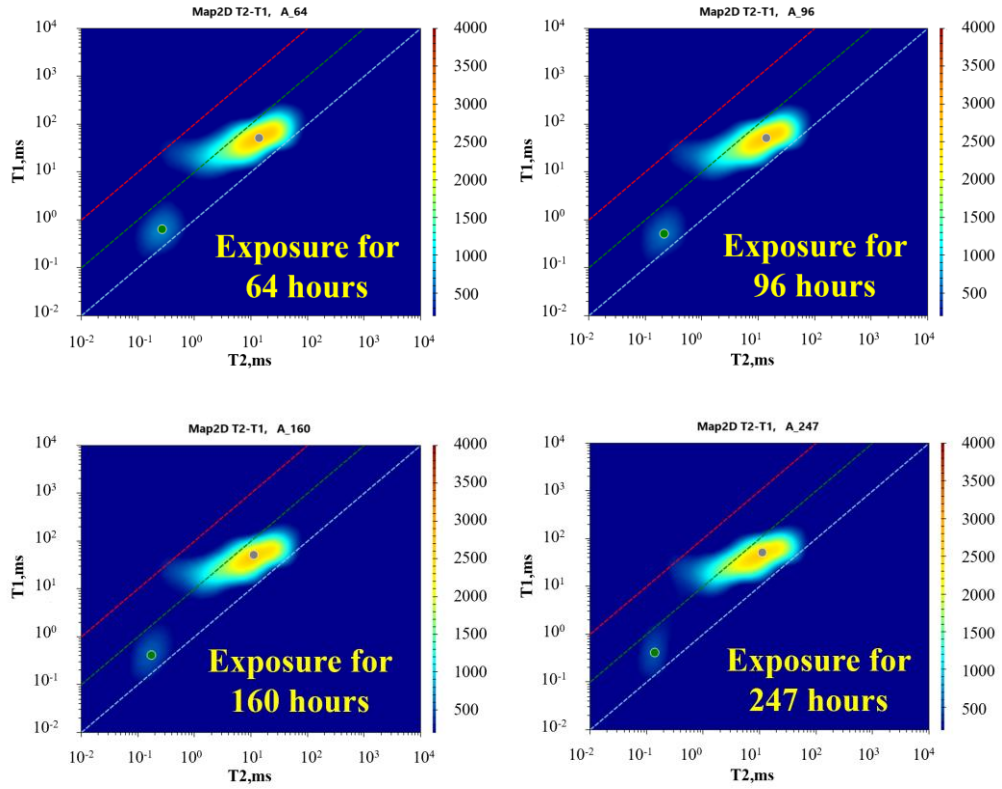

Figure 6. The results of twodimensional NMR experiments conducted at various dissipation stages of sample A.

5. Discussion

Different fluids exhibit distinct responses in the NMR T_1-T_2 distribution. As illustrated in Figure 7, the highlighted area in the lower-left corner represents the bounding water signal, while the highlighted area in the upper-right corner represents the crude oil signal. By integrating the signals from various regions of the two-dimensional distribution, the total intensity of different fluid signals can be determined [25]. The ratio of this intensity to the total signal intensity indicates the saturation of the respective fluids [24,26]. Therefore, changes in the signal amplitude of different fluid components in various regions of the NMR T_1-T_2 distribution at different dissipation times can reflect the changes in the content of these fluid components in the rock pores. For instance, in the NMR T_1-T_2 distribution of sample A (Figure 7), the boundaries of the two fluid components are delineated, with the crude oil component highlighted by a red box and the bounding water component highlighted by a yellow box. By calculating the signal amplitude ratio of the two regions and multiplying it by the current NMR-visible porosity, the remaining fluid content at different dissipation times can be assessed.

5.1. Bounding Water

Utilizing the method illustrated in Figure 7, the changes in bounding water fluid signals during the second dissipation stage are analyzed, and the results are presented in Table 2. In Sample A, the bounding water content decreases from 63.3% to 18.5%, while in Sample B, it decreases from 77.0% to 25.4%.

Table 2. The percentage change of bounding water fluid in the core with the dissipation time.

Sample	Permeability (mD)	4 h (%)	8 h (%)	16 h (%)	32 h (%)	64 h (%)	96 h (%)
A	18.724	63.3	52.4	41.9	34.5	21.7	18.5
B	34.972	77.0	67.3	53.9	43.3	30.4	25.4

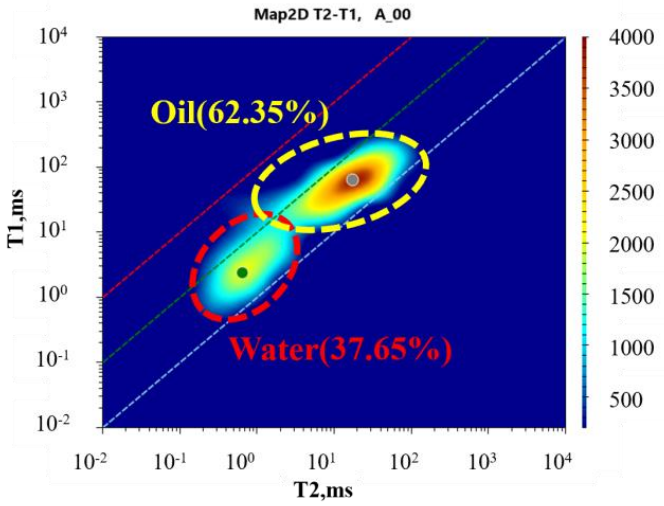

Figure 7. Schematic diagram of calculating the percentages of different fluid components using the twodimensional nuclear magnetic area integration method.

The bounding water content at different dissipation times is statistically analyzed and regression-fitted, as shown in Figure 8. The samples exhibit a strong logarithmic relationship, with the specific fitting formulas as follows:

$$\text{Sample A}: \ pw = -0.142ln(t) + 0.8236 \quad R^2 = 0.9953, \tag{6}$$

$$\text{Sample B}: \ pw = -0.166ln(t) + 1.0067 \quad R^2 = 0.9981, \tag{7}$$

where pw represents the remaining bounding water content, t denotes the dissipation time, and R signifies the fitting correlation coefficient, which exceeds 0.99, indicating high fitting accuracy. Furthermore, the initial bounding water content is influenced by the characteristics of the injected crude oil, particularly its viscosity. Low-viscosity crude oil, owing to its superior fluidity and smaller molecular size, displaces water more efficiently from small pores, resulting in reduced bounding water saturation.

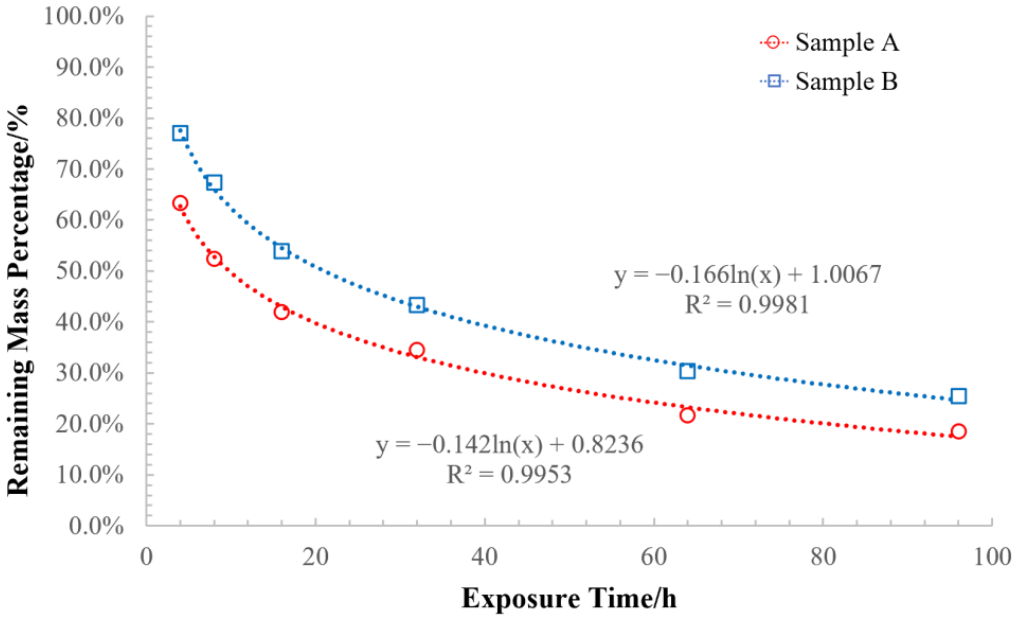

Figure 8. The relationship between the remaining mass percentage of irreducible water and exposure time.

5.2. Crude Oil of Different Viscosities

Utilizing the analytical methodology illustrated in Figure 6, the variations in crude oil signals throughout the second dissipation phase are examined, as shown in Table 3. The findings indicate that the residual crude oil content in the samples diminishes throughout the second dissipation phase, reflecting the dynamic alterations of crude oil components during dissipation, particularly the depletion of lighter components. This understanding is essential for comprehending the dissipation process of crude oil within geological formations.

Table 3. Percent change of crude oil in core with different dissipation times.

Sample	Oil Viscosity (mPas)	T2 Center (ms)	T1 Center (ms)	4 h (%)	8 h (%)	16 h (%)	32 h (%)	64 h (%)	96 h (%)
A	42	16.3	60.2	88.0	85.5	80.0	73.9	71.8	68.8
B	240	6.8	67.1	89.1	87.2	85.3	82.1	79.2	77.2

The proportion of residual crude oil content at various dissipation intervals is statistically analyzed and represented, as indicated by the dashed lines in Figure 9. The correlation between the proportion of residual crude oil content and dissipation time exhibits a strong logarithmic relationship.

$$\text{Sample A}: \ po = -0.063ln(t) + 0.9729 \quad R^2 = 0.9832 \tag{8}$$

$$\text{Sample B}: \ po = -0.038ln(t) + 0.9496 \quad R^2 = 0.9872 \tag{9}$$

where *po* denotes the residual crude oil content per unit volume, t represents the dissipation time, and R signifies the fitting correlation coefficient, exceeding 0.9. Subsequent analysis indicates that for Samples A and B, which possess similar porosity and permeability characteristics, as well as initial saturation states, the dissipation rate of the low-viscosity crude oil Sample A is markedly higher than that of the high-viscosity crude oil Sample B. By the conclusion of the second stage, the residual proportion of crude oil in sample A is considerably lower than that in sample B. This observation suggests a correlation between the dissipation process of crude oil and its viscosity, where increased viscosity results in slower dissipation.

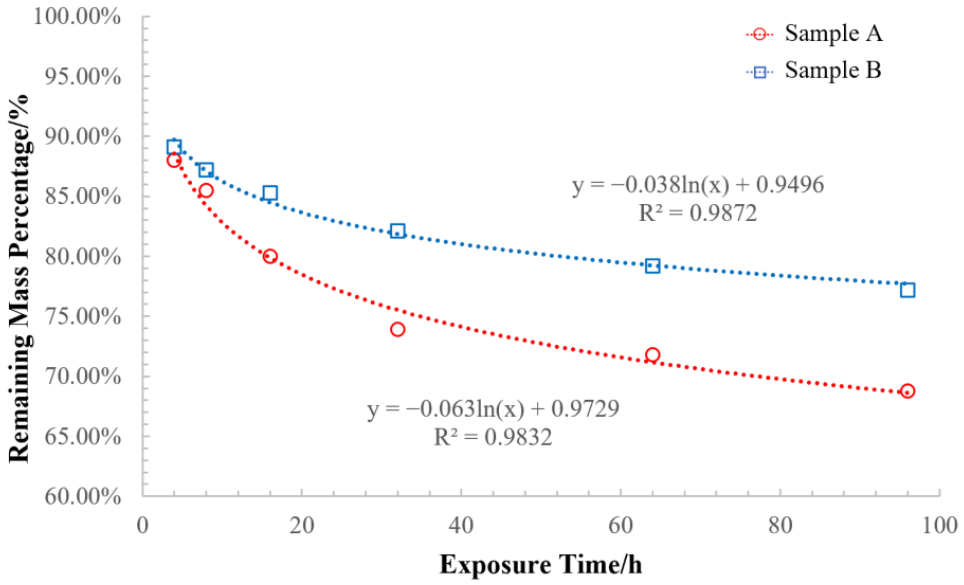

Figure 9. The relationship between the remaining mass percentage of crude oil and exposure time.

As shown in Figure 10, by comparing the changes in T_2 and T_1 values of crude oil components in the cores after 4 and 96 h of dissipation (see Table 4), it is observed that the T_2 values of crude oil components decreased, while the T_1/T_2 ratio markedly increased. This phenomenon indicates the depletion of lighter components in the crude oil, leading to decreased fluidity.

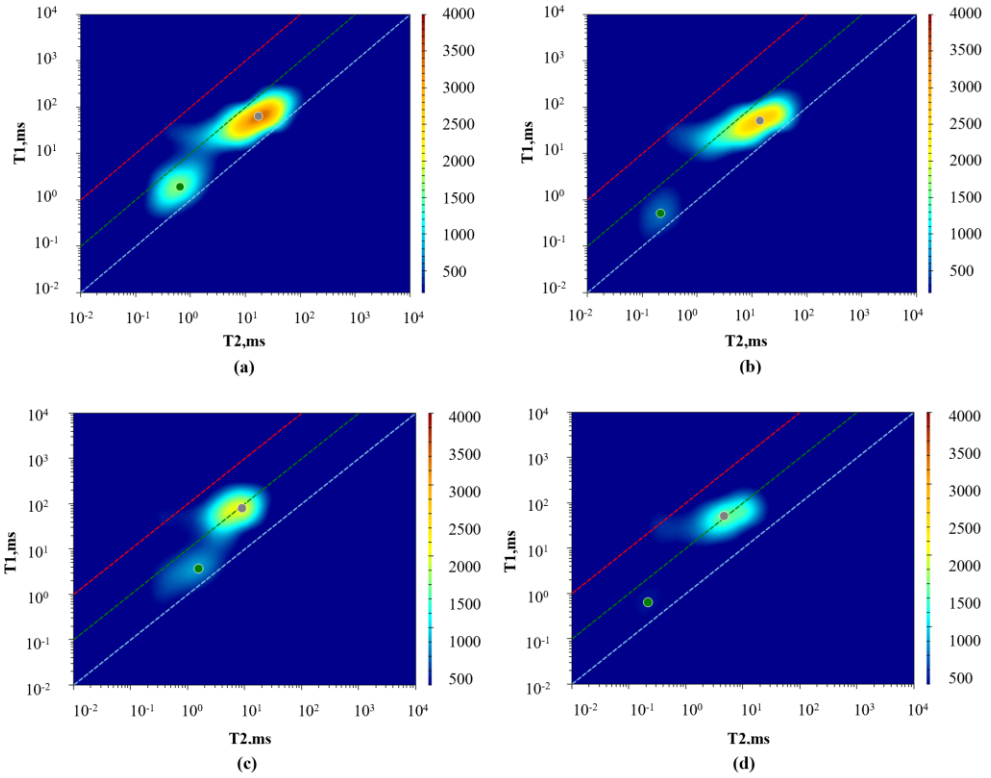

Figure 10. Two-dimensional NMR experimental results of each core fluid component in the second stage of fluid dissipation: (**a**) the NMR measurement result after 4 h of exposure treatment for Sample A; (**b**) the NMR measurement result after 96 h of exposure treatment for Sample A; (**c**) the NMR measurement result after 4 h of exposure treatment for Sample B; and (**d**) the NMR measurement result after 96 h of exposure treatment for Sample B.

Table 4. Changes in relaxation times of crude oil components in rock cores.

Sample	Oil Viscosity (mPas)	4-h T2 (ms)	4-h T1 (ms)	4-h T1/T2	96-h T2 (ms)	96-h T1 (ms)	96-h T1/T2
A	42	16.3	60.2	3.7	14.6	60.2	4.6
B	420	6.8	67.1	9.87	4.6	58.0	12.61

6. Conclusions

Through physical simulation experiments, the dissipation process of pore fluids within sandstone cores was investigated, elucidating the dissipation patterns of core pore fluids at various exposure durations.

(1) In the initial phase of exposing saturated cores, fluid dissipation predominantly occurs at the core surface. The fluid adhering to the surface rapidly dissipates into the atmosphere, resulting in a significant reduction in core weight. This process continues for approximately two hours.

(2) Following the loss of surface fluid, the fluid within the core transitions into a stable dissipation phase. During this phase, the dissipation rate of bounding water is markedly higher than that of crude oil. By the conclusion of the second phase, bounding water

is nearly entirely dissipated, leaving primarily crude oil. The dissipation rate of each fluid exhibits a logarithmic relationship with time, and this phase spans several hours to several tens of hours.

(3) The third phase constitutes the stabilization phase, commencing after 96 h. During this phase, crude oil within the core dissipates into the atmosphere at a reduced rate. This phenomenon arises due to the inherent differences in the physical and chemical properties of crude oil and bounding water. Bounding water, being less viscous and having smaller molecular size, can more readily diffuse through the interconnected pore network and evaporate.

(4) This study offers a qualitative reference for the dissipation patterns of fluids under ambient temperature conditions, focusing on sandstone cores saturated with crude oil of specific viscosity. To quantitatively assess the dissipation patterns of various lithologies and crude oils with differing viscosities under diverse temperature and humidity conditions, further comprehensive experimental research is necessary.

Author Contributions: The authors confirm their contributions to the paper as follows: Conceptualization and design, G.Z.; data collection, Z.L. and Y.M.; analysis and interpretation of results, G.Z., Z.L. and Y.M.; draft manuscript preparation, Z.L. All authors have read and agreed to the published version of the manuscript.

Funding: The authors received no specific funding for this study.

Institutional Review Board Statement: Not applicable.

Informed Consent Statement: Not applicable.

Data Availability Statement: The data presented in this study are available on request from the corresponding author. The data are not publicly available due to privacy.

Acknowledgments: The authors would like to thank the reviewers and academic editors for their useful suggestions for improving the quality of our manuscript.

Conflicts of Interest: The authors declare that they have no conflicts of interest to report regarding the present study.

References

1. Li, J.; Wang, M.; Li, J.; Zhao, X.; Hu, X.; Fu, A. Shale primary porosimetry based on 2D nuclear magnetic resonance of T1-T2. *Energy Geosci.* **2024**, *5*, 100270. [CrossRef]
2. Archie, G.E. The electrical resistivity log as an aid in determining some reservoir characteristics. *Trans. AIME* **1942**, *146*, 54–62. [CrossRef]
3. Fan, X.; Wang, G.; Dai, Q.; Li, Y.; Zhang, F.; He, Z.; Li, Q. Using image logs to identify fluid types in tight carbonate reservoirs via apparent formation water resistivity spectrum. *J. Pet. Sci. Eng.* **2019**, *178*, 937–947. [CrossRef]
4. Li, C.; Yan, W.; Wu, H.; Tian, H.; Zheng, J.; Yu, J.; Feng, Z.; Xu, H. Calculation of oil saturation in clay-rich shale reservoirs: A case study of Qing 1 Member of Cretaceous Qingshankou Formation in Gulong Sag, Songliao Basin, NE China. *Pet. Explor. Dev.* **2022**, *49*, 1351–1363. [CrossRef]
5. Timur, A. Effective porosity and permeability of sandstones investigated through nuclear magnetic principles. *Log Anal.* **1969**, *10*, 3–11.
6. de Freitas, K.L.F.; da Silva, P.N.; Faria, B.M.; Gonçalves, E.C.; Rios, E.H.; Nobre-Lopes, J.; Rabe, C.; Plastino, A.; Azeredo, R.B.d.V. A data mining approach for automatic classification of rock permeability. *J. Appl. Geophys.* **2022**, *196*, 104514. [CrossRef]
7. Heidary, M. An NMR-based model for determining irreducible water saturation in carbonate gas reservoirs. *J. Pet. Explor. Prod. Technol.* **2024**, *14*, 927–939. [CrossRef]
8. Guoqiang, L. Challenges and countermeasures of well logging data acquisition technology in unconventional petroleum exploration and development. *China Pet. Explor.* **2021**, *26*, 24.
9. Min, B.; Sondergeld, C.H.; Rai, C.S. Investigation of high frequency 1D NMR to characterize reservoir rocks. *J. Pet. Sci. Eng.* **2019**, *176*, 653–660. [CrossRef]
10. Valle, B.; Dal'Bó, P.F.; Santos, J.; Aguiar, L.; Coelho, P.; Favoreto, J.; Arena, M.; Santos, H.N.; Ribeiro, C.; Borghi, L. A new method to improve the NMR log interpretation in drilling mud-invaded zones: A case study from the Brazilian Pre-salt. *J. Pet. Sci. Eng.* **2021**, *203*, 108692. [CrossRef]
11. Anferova, S.; Anferov, V.; Arnold, J.; Talnishnikh, E.; Voda, M.A.; Kupferschläger, K.; Blümler, P.; Clauser, C.; Blümich, B. Improved Halbach sensor for NMR scanning of drill cores. *Magn. Reson. Imaging* **2007**, *25*, 474–480. [CrossRef]

12. Anferova, S.; Anferov, V.; Rata, D.G.; Blümich, B.; Arnold, J.; Clauser, C.; Blümler, P.; Raich, H. A mobile NMR device for measurements of porosity and pore size distributions of drilled core samples. *Concepts Magn. Reson. Part B Magn. Reson. Eng. Educ. J.* **2004**, *23*, 26–32. [CrossRef]
13. Arnold, J.; Clauser, C.; Pechnig, R.; Anferova, C.; Anferov, V.; Blümich, B. Porosity and permeability from mobile NMR core-scanning. *Petrophysics-SPWLA J. Form. Eval. Reserv. Descr.* **2006**, *47*.
14. Mardon, D.; Prammer, M.G.; Coates, G.R. Characterization of light hydrocarbon reservoirs by gradient-NMR well logging. *Magn. Reson. Imaging* **1996**, *14*, 769–777. [CrossRef]
15. Anand, V. Novel methodology for accurate resolution of fluid signatures from multi-dimensional NMR well-logging measurements. *J. Magn. Reson.* **2017**, *276*, 60–68. [CrossRef]
16. Song, Y.Q.; Venkataramanan, L.; Hürlimann, M.D.; Flaum, M.; Frulla, P.; Straley, C. T1-T2 correlation spectra obtained using a fast two-dimensional Laplace inversion. *J. Magn. Reson.* **2002**, *154*, 261–268. [CrossRef]
17. Sun, Y.; Zhai, C.; Xu, J.; Qin, L.; Tang, W. A method for accurate characterisation of the pore structure of a coal mass based on two-dimensional nuclear magnetic resonance T1–T2. *Fuel* **2020**, *262*, 116574. [CrossRef]
18. Li, J.; Jiang, C.; Wang, M.; Lu, S.; Chen, Z.; Chen, G.; Li, J.; Li, Z.; Lu, S. Adsorbed and free hydrocarbons in unconventional shale reservoir: A new insight from NMR T1-T2 maps. *Mar. Pet. Geol.* **2020**, *116*, 104311. [CrossRef]
19. Qin, Y.; Zhang, G.; Zhang, J.; Zhang, J.; Liu, Y.; Li, S. Study on the influence of magnetic field intensity on T2-T1 two-dimensional nuclear magnetic resonance experiment. *Prog. Geophys.* **2021**, *36*, 2082–2089.
20. Yue, Y.; Yidi, S.; Rui, G.; Lina, D.A.; Hou, J.; Yang, M. Determination of surface relaxivity for tight sandstone cores based on T2 cut-off value. *Pet. Geol. Exp.* **2022**, *44*, 342–349.
21. Telkki, V.V.; Urbańczyk, M.; Zhivonitko, V. Ultrafast methods for relaxation and diffusion. *Prog. Nucl. Magn. Reson. Spectrosc.* **2021**, *126*, 101–120. [CrossRef] [PubMed]
22. Qingfeng, D.; Shuai, H.; Chunyuan, G.; Feng, Y.; Dongshan, P.; Fan, J.; Peiqiang, Y. Study of micro flow visualization with nuclear magnetic resonance in core. *J. Exp. Fluid Mech.* **2016**, *30*, 98–103.
23. Mukhametdinova, A.; Habina-Skrzyniarz, I.; Krzyżak, A. NMR relaxometry interpretation of source rock liquid saturation—A holistic approach. *Mar. Pet. Geol.* **2021**, *132*, 105165. [CrossRef]
24. Fleury, M.; Romero-Sarmiento, M. Characterization of shales using T1–T2 NMR maps. *J. Pet. Sci. Eng.* **2016**, *137*, 55–62. [CrossRef]
25. Uskova, E.I.; Doroginitskii, M.M.; Skirda, V.D.; Fatkhutdinov, I.H. New Approach to Analyze 2D Map T1–T2. *Appl. Magn. Reson.* **2020**, *51*, 183–193. [CrossRef]
26. Ge, X.; Fan, Y.; Chen, H.; Deng, S.; Cao, Y.; Zahid, M.A. Probing the influential factors of NMR T1-T2 spectra in the characterization of the kerogen by numerical simulation. *J. Magn. Reson.* **2015**, *260*, 54–66. [CrossRef]